Paper 113

NONLINEAR WOODING–BINGHAM CONVECTION

D. Andrew S. Rees
Department of Mechanical Engineering, University of Bath,
Claverton Down, Bath BA2 7AY, United Kingdom.
Email: D.A.S.Rees@bath.ac.uk

ABSTRACT

The classical Wooding problem consists of a semi-infinite fluid-saturated porous medium which is bounded below by a heated horizontal surface with uniform transpiration into that surface (Wooding [1]). Thus the basic state which is analyzed for instability corresponds to a constant-velocity downward flow and an exponentially decaying temperature profile. Both the onset of convection and nonlinear flows have been the subject of many papers, and it is well-known that the onset of convection is subcritical; thus strongly nonlinear convection arises for a range of values of the Darcy-Rayleigh number which is below that given by linear theory.

In this paper we shall consider the modification to the Wooding problem which is brought about by replacing the Newtonian saturating fluid by a Bingham fluid. Bingham fluids have a yield stress but are otherwise Newtonian. Within the porous medium context, Pascal [2] suggested that Darcy's law is then replaced by the following Darcy-Bingham model:

$$u = \begin{cases} -\dfrac{K}{\mu}\Big[1 - \dfrac{G}{|p_x|}\Big]p_x & \text{when } |p_x| > G, \\ 0 & \text{otherwise,} \end{cases} \qquad (1)$$

where G is the threshold pressure gradient above which the fluid flows. The chief numerical difficulty associated with solving for the flow of a Bingham fluid in a porous medium is the presence of yield surfaces which separate regions of stagnation from regions where flow arises. This difficulty may be circumvented to a large extent by using a regularized version of the above Darcy-Bingham law which smoothes the discontinuities in the slope of u with respect to the applied pressure gradient, p_x (Rees [3]).

Numerical solutions of the Wooding-Bingham problem have been obtained using a second order accurate finite difference methodology with pseudo-timestepping. The presence of the yield surfaces, which mark the boundaries of stagnant regions, is modelled by means of a regularisation of the yield threshold. A linearised stability analysis is also presented. It is found that the primary effects of the presence of a yield threshold are (i) the appearance of stagnant regions around which the fluid flows and (ii) a modified solution curve where there are now two stable branches which are characterised by having different stagnation patterns.

INTRODUCTION

The flow of various types of non-Newtonian fluid within a porous medium is a well-established field of research, and is one with a variety of important applications, particularly in the oil industry. A Bingham fluid is characterized by having a yield stress, and therefore there is no rate of strain (i.e. no velocity gradient) when local stresses are less than that yield stress. When a porous matrix is absent this means that either the fluid is stagnant or else it acts like moving or rotating solid. In the context of a porous medium the equivalent situation is that there is a yield pressure gradient, or more generally, a yield value for the body forces such as buoyancy.

Pascal [2] was one of the first to write down the form of Darcy's law which may be applied when the porous medium is occupied by a Bingham fluid. The Pascal law states that the velocity is linearly dependent on the pressure gradient, but is zero when the absolute value of the pressure gradient lies below the yield gradient. More complicated laws may be derived if one considers porous media which are structured in some way, such as when taking the form of an ensemble of pipes or channels. Even in the most simple case, when the medium is composed of a periodic array of identical pipes, then the equivalent Darcy-Bingham law is a scaled form of the well-known Buckingham-Riener equation, for which the induced flow rises quadratically immediately post-threshold before becoming linear. More sedate post-threshold behaviour has been shown to apply when there are distributions of pipe radii/channel widths present; see Nash and Rees [3].

The present work is part of a programme looking at the effect of the presence of a yield threshold on convective flows within a porous medium. Previous works include free convective boundary layer

flows (Rees [4], Rees and Bassom [5,6]), and natural convection within differentially heated cavities (Rees [7,8]). In the cavity problems it was found that convection ensues when the Darcy-Rayleigh number, Ra, exceeds a critical value which dependent on both the Rees-Bingham number, Rb, and the aspect ratio of the cavity. The flow fields themselves, which are weaker than when the porous medium is occupied by a Newtonian fluid, are characterised by having stagnant regions around which the fluid moves.

Here we shall consider briefly the effect of a yield threshold on the Wooding problem, which is a mixed convection problem. The porous domain is semi-infinite, lying above a heated surface through which fluid is drawn. When the fluid is Newtonian, the onset of convection is well-known to be subcritical, and strongly convecting flows may be obtained at values of the Darcy-Rayleigh number which are below the critical value according to linearised stability theory. We shall present both a linear stability theory and some strongly nonlinear calculations. An *a priori* expectation was that the linearised stability theory would be identical to that for a Newtonian fluid because the presence of suction at the heated surface means that the yield threshold had already been overcome. A second expectation was that the solution curves would remain qualitatively the same as for the Newtonian case, but that the rationale for undertaking this work was to determine where stagnation would occur once the Darcy-Rayleigh number is large enough to produce an upward circulations which would cause a local negation of the effect of suction. It turned out that the two expectations were incorrect: the critical Rayleigh number does indeed depend on Rb, and the solutions curves change their shape markedly.

In successive sections we present the governing equations, formulate the linearised stability equations, discuss briefly the numerical method for nonlinear simulations, and give some conclusions. The present work, however, should be regarded an an initial exploratory study of the full Wooding-Bingham system, and therefore we shall confine ourselves to studying a region of horizontal width, 6, which is equivalent to the wavenumber $k = \pi/6 \simeq 0.523599$, a value which is just below the critical value for the classical Wooding problem with a Newtonian fluid; the reason for this choice is given below.

GOVERNING EQUATIONS

A suitably nondimensionalised form of the law of Pascal [2] for unidirectional and isothermal flow of a Darcy-Bingham fluid may be written in the form,

$$w = \begin{cases} -\left[1 - \dfrac{\mathrm{Rb}}{|p_z|}\right] p_z & \text{when } |p_z| > \mathrm{Rb}, \\ 0 & \text{otherwise,} \end{cases} \tag{2}$$

where z is the upward vertical coordinate and w is the corresponding velocity flux (see [7] for details). When buoyancy forces (subject to the Boussinesq approximation) are present this becomes,

$$w = -\Big[1 - \frac{\mathrm{Rb}}{|p_z - \mathrm{Ra}\,\theta|}\Big]\big(p_z - \mathrm{Ra}\,\theta\big), \tag{3}$$

when $|p_z - \mathrm{Ra}\,\theta| > \mathrm{Rb}$, and $w = 0$ otherwise. The corresponding Newtonian form is obtained when $\mathrm{Rb} = 0$. In this equation,

$$\mathrm{Ra} = \frac{\rho g \beta \Delta T K L}{\mu \alpha}, \qquad \text{and} \qquad \mathrm{Rb} = \frac{GKL}{\mu\alpha}, \tag{4}$$

are the Darcy-Rayleigh and Rees-Bingham numbers, respectively (see Rees [7]). Here L is a lengthscale which, in the absence of a scale such as the height of a layer, is taken to be α/W where α is the thermal diffusivity and W the downward suction velocity into the heated surface. In (4) most of the terms correspond to their usual definitions in the porous medium context, but G is the yield pressure gradient.

As with Bingham fluid flows n the absence of a porous matrix, simulations are made complicated by the need to determine where the yield surface is. Here we shall use a regularisation which has some similarity to that of Papanastasiou [9] to soften the effect of the yield threshold. This is equivalent to the fluid having an artifically high viscosity when the body forces are small. This allows for a smooth transition between stagnation and strong flow. We shall replace Eq. (2) by,

$$w + \mathrm{Rb}\tanh(cw/\mathrm{Rb}) = -p_z + \mathrm{Ra}\,\theta, \tag{5}$$

where c is an adjustable parameter. Pascal's threshold model may be seen to be recovered when $c \to \infty$ in Fig. 2 of [7]. When w is sufficiently small, the left hand side of Eq. (5) takes the form, $(1 + c)w$, and therefore this is equivalent to a fluid with viscosity $(1 + c)\mu$.

The equivalent frame-invariant system for isotropic two-dimensional convection is,

$$\Big[1 + \mathrm{Rb}\,\frac{\tanh(cq/\mathrm{Rb})}{q}\Big]u = -p_x, \tag{6}$$

$$\Big[1 + \mathrm{Rb}\,\frac{\tanh(cq/\mathrm{Rb})}{q}\Big]w = -p_z + \mathrm{Ra}\,\theta, \tag{7}$$

where the value, q, is given by,

$$q^2 = u^2 + w^2. \tag{8}$$

The streamfunction is given by $u = -\psi_z$ and $w = \psi_x$, and therefore the regularised momentum equation is found to be,

$$\nabla^2\psi + \frac{\mathrm{Rb}\,\tanh(cq/\mathrm{Rb})}{q^3}\left[\psi_z^2\psi_{xx} - 2\psi_x\psi_z\psi_{xz} + \psi_x^2\psi_{zz}\right] + \frac{c\,\mathrm{sech}^2(cq/\mathrm{Rb})}{q^2}\left[\psi_x^2\psi_{xx} + 2\psi_x\psi_z\psi_{xz} + \psi_z^2\psi_{zz}\right] = \mathrm{Ra}\,\theta_x, \tag{9}$$

where $q^2 = \psi_x^2 + \psi_y^2$. Possible singular behaviour when q is small is obviated by using a five-term Maclaurin series in q when $q < 10^{-4}$. Finally, the heat transport equation takes its usual form:

$$\theta_t = \nabla^2\theta + \psi_z\theta_x - \psi_x\theta_z. \tag{10}$$

The boundary conditions for this numerical problem are given by the following:

$$z = 0: \qquad \psi = -x, \quad \theta = 1 \tag{11}$$

$$z \to \infty: \qquad \psi \to -x, \qquad \theta \to 0; \tag{12}$$

the conditions for ψ are equivalent to $w = -1$.

The basic flow whose stability we shall analyse may easily be verified to be

$$\psi = -x, \qquad \theta = e^{-z}. \tag{13}$$

The presence of surface suction means that there is a balance between upward conduction and downward advection that makes the thermal region to be of boundary layer type.

LINEAR STABILITY ANALYSIS

We shall perturb the basic solution given in (13) by setting

$$\psi = -x + \Psi, \qquad \theta = e^{-z} + \Theta \tag{14}$$

into Eqs. (9) and (10), and neglecting all nonlinear terms in the perturbations. Thus we obtain,

$$\nabla^2\Psi + \mathrm{Rb}\,\tanh\left(\frac{c}{\mathrm{Rb}}\right)\Psi_{zz} + c\,\mathrm{sech}^2\left(\frac{c}{\mathrm{Rb}}\right)\Psi_{xx} = \mathrm{Ra}\,\theta_x, \tag{15}$$

$$\Theta_t = \nabla^2\Theta + \Theta_z + e^{-z}\Theta_x. \tag{16}$$

In practice (see later) the values of c/Rb will be large enough that the tanh and sech^2 functions in (15) may be replaced with 1 and 0 with very high accuracy. Therefore Eq. (15) may be replaced by,

$$\Psi_{xx} + (1 + \mathrm{Rb})\Psi_{zz} = \mathrm{Ra}\,\theta_x. \tag{17}$$

We see, therefore, that the presence of the yield threshold causes the linear stability problem to be anisotropic, and therefore the linearised theory for a Bingham fluid differs from that of a Newtonian fluid even though the yield threshold has been exceeded and the Darcy-Bingham law is linear within this regime.

Monochromatic disturbances may now be considered by using the substitutions,

$$\Psi = f(z)\sin kx, \qquad \Theta = g(z)\cos kx, \tag{18}$$

and this yields the following ordinary differential eigenvzlue problem for the Darcy-Rayleigh number in terms of k and Rb:

$$(1 + \mathrm{Rb})f'' - k^2 f + \mathrm{Ra}\,kg = 0, \tag{19}$$

$$g'' + g' - k^2 g + e^{-z}kf = 0, \tag{20}$$

which is to be solved subject to

$$z = 0: \quad f = g = 0, \qquad z \to \infty: \quad f, g \to 0. \tag{21}$$

These equations were solved using a standard 4th order Runge-Kutta scheme with the shooting method where the additional normalisation condition, $g'(0) = 1$, was applied in order to ensure nonzero solutions, and where an extra first order equation, $\mathrm{Ra}' = 0$, was added to the system — this is a standard method for solving ordinary differential eigenvalue problems. Details of the numerical results will be presented below.

NUMERICAL METHOD

Equations (9) and (10) subject to the boundary conditions given in (11) and (12) were approximated using second order accurate central differences in space. We adopted a pseudo time-stepping methodology in order to reduce substantially the code development time, and therefore the extra term, ψ_t, was added to the right hand side of Eq. (9). Then timestepping for both the momentum and heat transport equations was achieved using the DuFort-Frankel method. While this gives an incorrect evolution in time, any steady-state solution which is achieved is a genuine steady-state solution.

As this is an initial study of what could well be a somewhat complicated system, our numerical simulations have been confined to having one convecting cell within a domain of width, 6. We have also chosen to use $z_{\max} = 36$, which is sufficient to contain the both the velocity and temperature fields when the fluid is Newtonian and when $Ra \leq 30$. A uniform numerical grid with 32×192 intervals was used with

a timestep of 0.01. We chose to use $c = 20$ as the regularisation constant, and therefore the effective viscosity of the fluid within a "stagnant" region is 21 times that when the fluid is well within the nonstagnant regime.

Computations were either initiated at $t = 0$ using disturbances of the form,

$$\psi = -x, \qquad \theta = e^{-z} + Ae^{-z}\cos kx, \qquad (22)$$

where the amplitude, A, took various values, or, when a sequence of computations were performed, the solution at one value of Ra was used as the initial profile at the next value of Ra in the sequence. In this way we were able construct all the possible steady solutions. We have confined our studies to $0 < \mathrm{Ra} < 40$ and to those cases where the maximum value of the disturbance streamfunction (i.e $\psi + x$) is less than 8; this was found to guarantee that our solutions lay well within the computational domain in the z-direction.

NUMERICAL SOLUTIONS

Context: The Newtonian context of the present work is shown in Fig. 1 where both linear and nonlinear solution curves are shown for a Newtonian fluid; this Figure is taken from Rees [10].

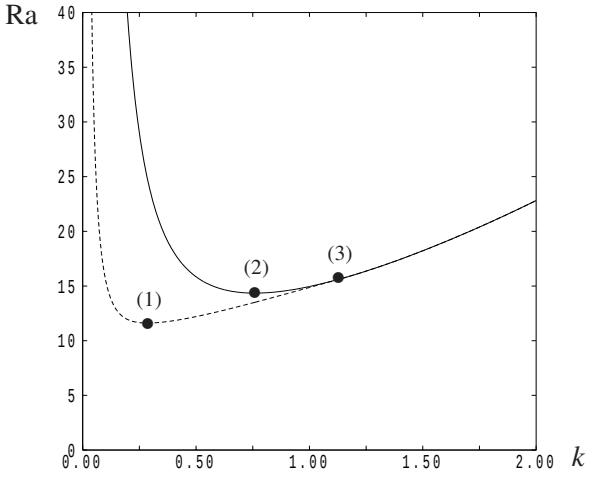

Figure 1.
The linear (continuous) and nonlinear (dashed) neutral curves. (1) nonlinear onset; (2) linear onset; (3) the transition between subcritical and supercritical onset.

For a Newtonian fluid ($\mathrm{Rb} = 0$) the onset of convection takes place at $\mathrm{Ra} = 14.3552$ when $k = 0.7589$, using linearised theory, whereas the most subcritical nonlinear solution arises when $\mathrm{Ra} = 11.6132$ when $k = 0.2867$. The linear and nonlinear curves merge when $\mathrm{Ra} = 15.6308$ and $k = 1.1320$. Therefore the onset of convection is supercritical when $k > 1.1320$ but is subcritical otherwise. The wavenumber we have chosen to study, $k = \pi/6 = 0.523599$, is roughly in the middle of these two critical wavenumbers. This value means that there is quite a large degree of subcriticality, at least for the convection of a Newtonian fluid, and more so than if we had chosen to confine our studies to the critical value from linear theory.

Onset according to linearised theory: Figure 2 displays how the critical value for Ra varies with strength of the yield threshold, Rb.

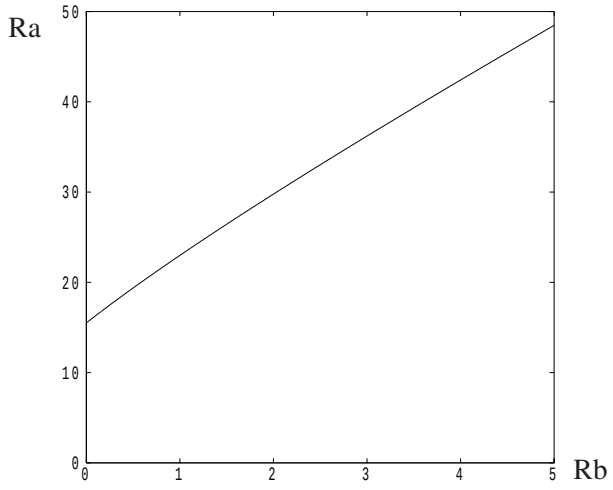

Figure 2.
The variation of the critical value of Ra as a function of Rb when $k = \pi/6$.

When $\mathrm{Rb} = 0$ we recover $\mathrm{Ra} = 15.5125$, the value for a Newtonian fluid at $k = \pi/6$. However, as Rb increases, the critical value of Ra also increases and this increase is not quite linear. If one didn't have sight of Eq. (19), it might seem evident that the critical value of Ra would not depend on Rb given that the yield threshold has already been exceeded by the strength of the vertical pressure gradient which draws the fluid through the heated surface. However, the fact that there isn't a direct proportionality between the induced flow and the applied pressure gradient means that the existence of the yield threshold induces an anisotropy, which is reflected in the different coefficients of the two diffusion terms in Eq. (17).

Solution curves: Figure 3 displays solution curves as a function of Ra for $\mathrm{Rb} = 0$, 0.5, 1, 1.5, 2, 2.5 and 3. These curves use the maximum value of $\psi_{\mathrm{pert}} = \psi + x$, denoted by $\psi_{\mathrm{pert}}^{\mathrm{max}}$, as a proxy for the strength of the induced convection. Newtonian fluid corresponds to $\mathrm{Rb} = 0$ and the shape of the solution curve is consistent with current knowledge: the onset of convection is subcritical, but eventually the solution curve

bends back towards larger values of Ra. Thus the first appearance of convection is strongly nonlinear. It is important to note that continuous lines correspond to solutions which have been computed using our pseudo-timestepping method, and we presume that all such solutions will be stable in practice. Pseudo-timestepping methods are unable to compute solutions which are temporally unstable, and therefore the dotted lines shown in Fig. 3 are cubic curves which have been used to connect the computed turning points on the stable branches with the critical values of Ra which were obtained from the earlier linearised stability analysis. Thus the dotted curves represent the true solution curves qualitatively, but not quantitatively. A more sophisticated numerical scheme is needed to compute the unstable branches.

However, as Rb increases, this familiar subcritical shape is modified into a new form in which there are two unstable branches which link two stable branches and the zero solution. This makes for an interesting change in the hysteretical properties of the solutions which would appear in practice as Ra is varied and if we assume that there are always very small amplitude disturbances present. In all the Rb $\neq 0$ cases shown, the zero-solution remains stable up to the critical value of Ra, whereupon solutions transfer immediately to the upper stable solution branch. On the other hand, as Ra decreases from sufficiently large values, the upper stable branch remains the favoured solution until the turning point is encountered. Thereafter the solution drops to the lower stable branch, and, for a slightly smaller value of Ra, even this solution is extinguished and disturbances decay to zero.

The contours in Figs. 4 and 5 use 20 equal intervals between the respective extrema of the streamfunction and temperature fields. In the latter case the extrema are 0 and 1, but in the former case the minimum is always -6 whereas the maximum depends on whether there is a recirculation near the bottom left hand region. If not, then the maximum is 0, but if there is, then the maximum is a positive value. This is why there appears to be more closely-spaced streamlines in the two left hand frames of each figure (which correspond to the lower stable branches in Fig. 3) than in the remaining three frames (which correspond to the upper stable branches). The flows at $z = 36$ for all 10 frames in these figures are essentially identical.

It is also clear from Fig. 3 that the depth of subcriticality (i.e. the difference between Ra_c and the smallest value of Ra for which there is a nonzero solution) increases as Rb increases.

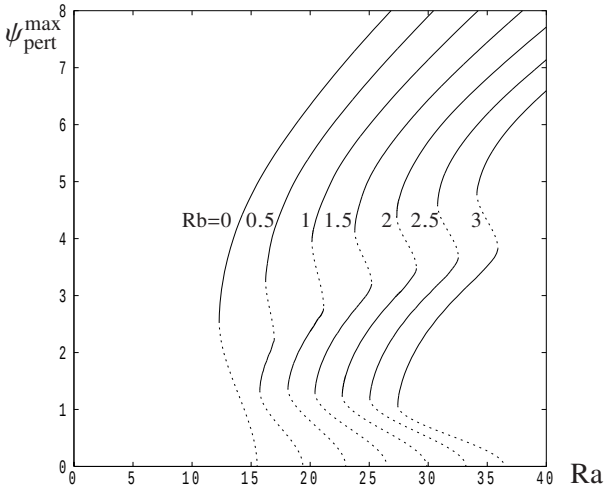

Figure 3.
Solution curves for Rb = 0, 0.5, 1, 1.5, 2, 2.5 and 3. Continuous lines represent computed stable solutions. Dashed lines represent the qualitative behaviour of the connecting unstable branches.

Streamlines and isotherms: The natural question which follows the discovery of two stable branches, when there was only one when the fluid is Newtonian, is: what is the difference between the flows which are represented by these branches? This is answered in Figs. 4 and 5 where we depict streamlines, isotherms and stagnant regions for a selection of values of Ra and Rb.

The basic temperature field which is given by Eq. (13) is approximately what may be seen on the right hand side of the Ra = 18 frame in Fig 4. The uppermost contour (which corresponds to $\theta = 0.05$) may be seen to be at a distance of roughly $z = 3$. This boundary layer thickness serves as a reference for the amount of deformation suffered by the temperature field when convection becomes strong. In both Figs 4 and 5 it is seen clearly that the spatial extent of the temperature field increases rapidly as the Darcy-Rayleigh number increases. The main physical reason for this is that, while inflow towards the $z = 0$ boundary will make the hot region narrower locally, outflow is unrestrained due to the absence of an outer boundary and heat is advected away from the hot surface. Our earlier statement about the present choice of the value of $z_{\max}$ and the range of values for Ra which has been considered is vindicated by the fact that the temperature field only just fits into the computational domain for the largest values of Ra used in these Figures.

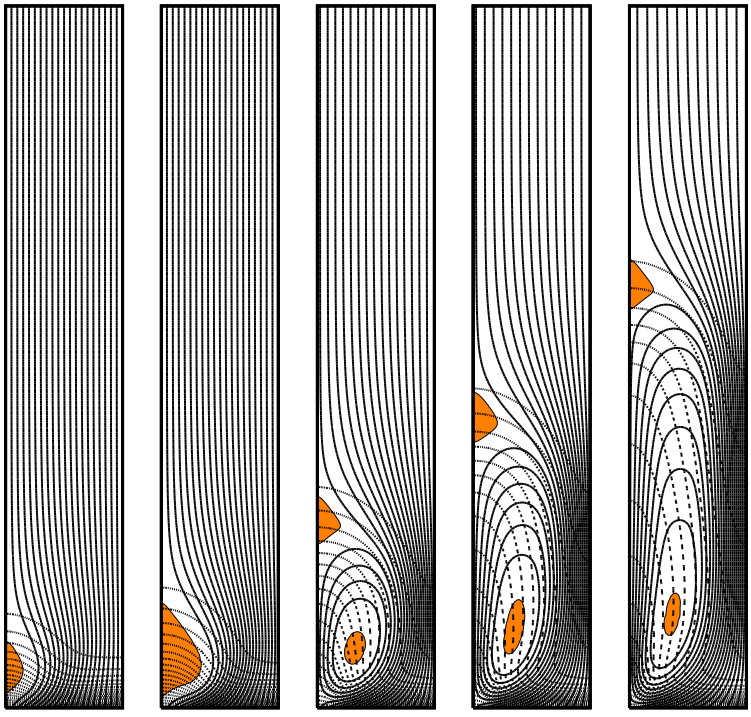

Figure 4.
Streamlines (continuous lines), isotherms (dashed lines) and stagnant regions (coloured orange) for the given values of Ra when Rb = 1.

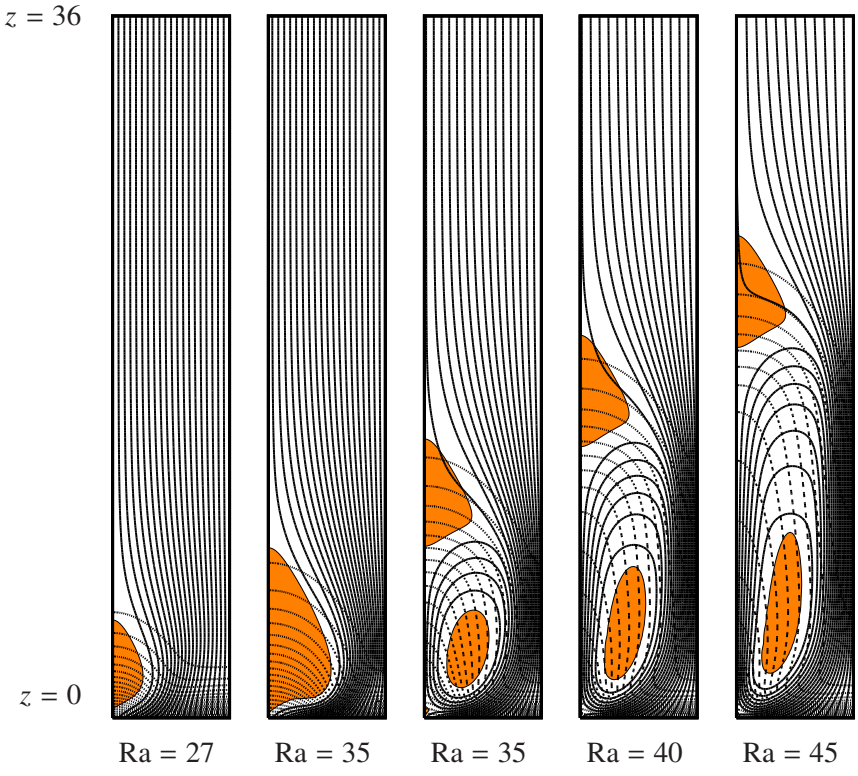

Figure 5.
Streamlines (continuous lines), isotherms (dashed lines) and stagnant regions (coloured orange) for the given values of Ra when Rb = 3.

In both Figs. 4 and 5, the two left-hand frames, which are lower branch solutions, are characterised by having only one stagnant region. Thus the inflow from infinity has to squeeze past that stagnant region, and therefore only conduction may take place within it. On the other hand, the remaining frames, which are upper branch solutions, are characterised by having two stagnant regions. One of these is the centre of a strongly convecting cell (which is a common feature for Darcy-Bingham flows; see [7,8]), while the other is centred on where the $\psi = 0$ contour reattaches onto the left hand boundary. Clearly the flow patterns (and hence the stagnant regions themselves) are very different between the upper and lower branches of Fig. 3. As it is a tenet of bifurcation theory that no solution branch can terminate, the dashed lines shown in Fig. 3 must exist as possible steady if unstable solutions of the full governing equations. It will be on these dashed lines that one flow pattern will morph gradually into the other; it is hoped to report on this at a later date — such unstable solutions can only be computed using a more sophisticated numerical scheme than we have employed here.

CONCLUSIONS

We have sought to determine how the presence of a yield stress in an otherwise Newtonian fluid which saturates a porous medium alters the behaviour of convective instability in the well-known Wooding problem. Although the suction at the heated surface and the presence of a uniform flow into that surface means that the yield threshold has already been exceeded, we have found two that strong effects are present. The first is that the linear stability threshold changes and that the critical value of the Darcy-Rayleigh number for instability increases with Rb. The second is that the familiar subcritical instability of a Newtonian fluid, the solution curve for which has one turning point, now has three turning points and two stable solution branches. Regions of overlap in terms of a range of values of Ra arise and clearly, then, the solution which appears in practice will depend very much on the nature of the perturbation.

All of the above occurs when $k = \pi/6$ and therefore it is not possible at this stage to confirm that the behaviours we have uncovered are global, but by continuity they will also arise for a range of values of k about $\pi/6$.

REFERENCES

1. Wooding, R.A. (1960) Rayleigh instability of a thermal boundary layer flow through a porous medium, *J. Fluid Mech.*, Vol. 9, pp. 183-192.
2. Pascal, H. (1981) Nonsteady flow through porous media in the presence of a threshold gradient, *Acta Mechanica*, Vol. 39, pp. 207-224.
3. Nash, S., Rees, D.A.S. (2017) The effect of microstructure on models for the flow of a Bingham fluid in porous media, *Transport in Porous Media*, Vol. 116, pp. 1073-1092.
4. Rees, D.A.S. (2015) On convective boundary layer flows of a Bingham fluid in a porous medium, *Int. J, Heat Mass Transfer*, Vol. 82, pp. 206-212.
5. Rees, D.A.S., Bassom, A.P. (2015) Unsteady thermal boundary layer flows of a Bingham fluid in a porous medium, *International Journal of Heat and Mass Transfer*, Vol. 82, pp. 460-467.
6. Rees, D.A.S., Bassom, A.P. (2016) Unsteady thermal boundary layer flows of a Bingham fluid in a porous medium following a sudden change in surface heat flux, *International Journal of Heat and Mass Transfer*, Vol. 93, pp. 1100-1106.
7. Rees, D.A.S. (2016) The convection of a Bingham fluid in a differentially-heated porous cavity, *Int. Journal Num. Methods Heat Fluid Flow*, Vol. 26, pp. 879-896.
8. Rees, D.A.S. (2017) Convective flow of a Bingham fluid in an internally-heated porous enclosure, *Paper 189 at CHT17, the 6th International Symposium on Advances in Computational Heat Transfer, Naples, Italy. May 2017.*
9. Papanastasiou, T.C. (1987) Flow of materials with yield, *Journal of Rheology*, Vol. 31, pp. 385-404.
10. Rees, D.A.S. (2009) The onset and nonlinear development of vortex instabilities in a horizontal forced convection boundary layer with uniform surface suction, *Transport in Porous Media [R.A.Wooding Special Issue]*, Vol. 77, pp. 243-265.